Biol Cybern (2012) 106:573–585
DOI 10.1007/s00422-011-0460-8

ORIGINAL PAPER

Biological Cybernetics

Using individual-muscle specific instead of across-muscle mean data halves muscle simulation error

Marcus Blümel · Christoph Guschlbauer · Scott L. Hooper · Ansgar Büschges

Received: 13 June 2011 / Accepted: 10 October 2011 / Published online: 7 November 2012

Abstract Hill-type parameter values measured in experiments on single muscles show large across-muscle variation. Using individual-muscle specific values instead of the more standard approach of across-muscle means might therefore improve muscle model performance. We show here that using mean values increased simulation normalized RMS error in all tested motor nerve stimulation paradigms in both isotonic and isometric conditions, doubling mean simulation error from 9 to 18% (different at $p < 0.0001$). These data suggest muscle-specific measurement of Hill-type model parameters is necessary in work requiring highly accurate muscle model construction. Maximum muscle force (F_{max}) showed large (fourfold) across-muscle variation. To test the role of F_{max} in model performance we compared the errors of models using mean F_{max} and muscle-specific values for the other model parameters, and models using muscle-specific F_{max} values and mean values for the other model parameters. Using muscle-specific F_{max} values did not improve model performance compared to using mean values for all parameters, but using muscle-specific values for all parameters but F_{max} did (to an error of 14%, different from muscle-specific, mean all parameters, and mean only F_{max} errors at $p \leq 0.014$). Significantly improving model performance thus required muscle-specific values for at least a subset of parameters other than F_{max}, and best performance required muscle-specific values for this subset and F_{max}. Detailed consideration of model performance suggested that remaining model error likely stemmed from activation of both fast and slow motor neurons in our experiments and inadequate specification of model activation dynamics.

Keywords *Carausius morosus* · Stick insect · Invertebrate

M. Blümel · C. Guschlbauer · S. L. Hooper (✉) · A. Büschges
Zoologisches Institut, Universität zu Köln, Cologne, Germany
e-mail: hooper@ohio.edu

S. L. Hooper
Neurobiology Program, Department of Biological Sciences,
Ohio University, Athens, OH, USA

M. Blümel
e-mail: bluemelm@uni-koeln.de

C. Guschlbauer
e-mail: guschlbauer@uni-koeln.de

A. Büschges
e-mail: Ansgar.Bueschges@uni-koeln.de

List of symbols

a, b	Terms in low pass filter (Eqs. 1, 2)
A, B	Terms in FV equations (Eqs. 11, 13)
A_{act}	Maximum amplitude of force–length curves (Eqs. 5, 8, 9)
act	Muscle activation (Eqs. 1, 3, 10–14)
c_{neg}, c_{pos}	Curvatures of Hill hyperbola for shortening (Eq. 11) and lengthening (Eq. 13) contractions, respectively
$curv_{\omega}$	Curvature of hyperbola relating ω and *act* (Eq. 10)
filter	Decay amplitude per time step in low pass filter (Eqs. 2–4)
F_L	Active force at different muscle lengths (force–length curve) (Eqs. 5, 8, 14)
F_P	Steady-state passive force (parallel spring) (Eqs. 7, 14)
F_{SE}	Series elastic spring force (Eq. 6)
F_V	F_L at different contraction velocities (force–velocity curve) (Eqs. 11, 13, 14)
k_1, k_2	Passive steady-state force–length curve constants (Eq. 7)

k_3	Proportionality constant in quadratic force equation (Eq. 6)
L_{CE}	Contractile element length (which equals parallel elastic length) (Eqs. 7, 8, 14)
L_M	Muscle length (Eq. 5)
L_{SE}	Series elastic element length (Eq. 6)
n	Simulation time step number (Eqs. 1, 3)
scaling	Scaling factor in low pass filter (Eq. 3)
t_{const}	Time constant in seconds of low pass filter (Eq. 4)
v	Velocity of muscle length change (Eqs. 11, 13, 14)
$v_{max\ neg}$, $v_{max\ pos}$	Maximum velocity of muscle length change for shortening (Eqs.11, 12) and lengthening (Eq. 13) contractions, respectively
$v_{max\ (act=1)}$	$v_{max\ pos}$ at an activation of 1 (Eq. 12)
ω	"Length" frequency of force–length curves (Eqs. 5, 8–10)
x	Stimulation input level in low pass filter (Eqs. 1, 3)

1 Introduction

Muscles transform motor neuron firing into force and movement, and hence play a central role in the production of behavior. Many models predicting muscle force and length changes in response to motor neuron activity have therefore been developed. These models require describing multiple properties (e.g., series and parallel passive elasticities, force–length, and force–velocity curves), many of which depend on multiple parameters. The values of all these parameters are typically not measured simultaneously in experiments on single muscles. Instead one or a few parameters are measured in experiments on muscles from several individual animals, another set of parameters from muscles from other individuals, etc., and these across-animal data are then averaged to obtain mean values for each parameter. This approach has a potential difficulty because of the large number of these parameters and because we have shown that most of them show large across-individual variation and assort independently (Blümel et al. 2012a,b). In any individual muscle it is therefore unlikely that the values of all these parameters will be near the population means (see Langlois and Roggmann 1990; Golowasch et al. 2002, for discussions of this concern using human beauty and neuron membrane conductances as examples). Simulations using mean values would thus likely represent only a small minority of real muscles.

Testing whether this issue causes significant error requires measuring all a muscle's defining parameters in single experiments. We developed techniques to achieve this goal with the stick insect (*Carausius morosus*) extensor tibiae muscle (Blümel et al. 2012a). We show here that muscle-specific models reproduce muscle responses to tonic and physiological motor neuron driving approximately 50% more accurately than models using across-individual mean parameter values. The maximum force the muscles can produce (F_{max}) showed wide across-muscle variation, is easy to measure, and would be expected to be strongly affected by life history. We therefore tested if using muscle-specific F_{max} values would improve simulation performance above using all parameter means. However, muscle-specific F_{max} simulations were no more accurate than all-mean simulations. Most accurate modeling of extensor (and hence possibly other) muscles therefore requires muscle-individual measurement of F_{max} and at least a subset of the other muscle-defining parameters.

2 Materials and methods

2.1 Experiment and simulation conditions

We performed experiments and simulations in isometric and isotonic conditions. The extensor muscle motor nerve (nl3) was stimulated with four constant frequency pulse trains (40, 60, 80, and 100 Hz, each for 1 s) or a series of pulses delivered in the same patterns as fast extensor tibiae motor neuron firing during stick insect sideways stepping (physiological stimulation; for detailed experimental methods see Blümel et al. 2012a). Three physiological patterns, all recorded from the same animal (see Fig. 2A in Hooper et al. 2006), were applied. Physiological pattern 1 consisted of a single step, pattern 2 of two sequential steps, and pattern 3 of three sequential steps. Isotonic measurements and simulations were conducted only with physiological stimulations. Our data set therefore contains three stimulation paradigms: isometric contractions with fixed frequency stimulations, isometric contractions with physiological stimulation, and isotonic contractions with physiological stimulation. Data from only nine muscles (not ten as in Blümel et al. 2012a,b) are presented here because the contractions of one of the muscles were too weak to shorten against the 40 mN counterforce used in our isotonic contractions.

2.2 General approach

Performing muscle simulations required adding activation and mechanical simulation modules (Sects. 2.3, 2.4) to our Hill-type model (Blümel et al. 2012a) (see Fig. 2). The activation module converted discrete spike patterns into a continuous activation level. The mechanical module modeled how the contractile element and series and parallel spring components responded to changes in activation and external force. The Hill model predicted muscle force from activa-

tion level and contractile and spring component length and velocity (for a review see Winters 1990).

2.3 Activation module

In Blümel et al. (2012a,b) the values of the parameters in the equations defining muscle activation were measured at steady-state levels of muscle contraction. This work thus did not describe how muscle activation changes over time in response to motor neuron input. We wanted here to compare muscle contraction and simulation output across time. It was therefore necessary to model how muscle activation changes with time in response to motor neuron activity. Multiple models of muscle activation exist, perhaps most prominent those of Zajac (1989) and Hatze (1977, 1978), many of which are quite complex (e.g., Zakotnik et al. 2006). Complex activation is powerful, but also tends to subsume Hill-model components. Because our Hill-model is well-defined and based on experimental data, we wanted to maintain it in its full form and keep it distinctly separate from the model's activation component. We therefore wanted to model activation responses to motor neuron input as simply as possible.

Low pass filtering reproduces many aspects of stick insect muscle isometric responses to motor neuron input (Hooper et al. 2007). We therefore modeled activation with a single-pole, first-order low-pass filter. The standard recursion equation (Smith 1997) for such a filter is

$$act[n] = a \cdot x[n] + b \cdot act[n-1] \tag{1}$$

where n is model present time step, $act[n]$ is muscle present activation, $x[n]$ is present stimulation input level (a value of 1 during a motor neuron spike, 0 otherwise), $act[n-1]$ is muscle activation one time step before the present, and a and b are recursion coefficients. In a low-pass filter a and b can be replaced by two equations with a single parameter (here called *filter*)

$$\begin{aligned} a &= 1 - filter \\ b &= filter \end{aligned} \tag{2}$$

where *filter* sets the decay amplitude per time step and varies between zero and one. The other component of the activation module was a scaling factor (*scaling*) that multiplied the input $x[n]$ by a constant. The complete activation equation was thus

$$\begin{aligned} act[n] = (1 - filter) \cdot (scaling \cdot x[n]) \\ + filter \cdot act[n-1] \end{aligned} \tag{3}$$

The time constant of the filter described by Eq. 3 depends on time step duration because *filter* is the amount of decay that occurs each time step, and the number of time steps that occur per second depends on time step duration. The following equation can be used to convert the *filter* values presented here (see Fig. 4a) to time constants that are independent of simulation time step duration:

$$t_{\text{const}} = -\Delta t / \ln(filter) \tag{4}$$

where t_{const} is the time constant (the duration in which the output signal will decay by $1/e$) in seconds and Δt is time step duration, 0.001 s in all simulations used here.

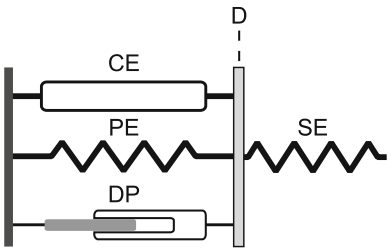

Fig. 1 Model components and arrangement. The model consisted of parallel contractile (CE), elastic (PE), and damping (DP) elements in series with an elastic element (SE). The *line* between the parallel elements and the SE element is labeled 'D'. In the text SE length is abbreviated 'L_{SE}' and the lengths of the parallel elements (all of which must be always equal) 'L_{CE}'

2.4 Mechanical simulation

Calculating muscle force and length changes requires choosing a particular arrangement of model components. We chose here a standard arrangement consisting of a contractile element (CE) in parallel with an elastic element (PE), with both elements in series with another elastic element (SE) (Fig. 1). In Blümel et al. (2012a,b) we presented a set of equations and parameter values that describe various real muscle properties. These measurements were purposefully chosen to be model independent, and in particular were generally expressed in terms of total muscle length (L_{M}). Correctly implementing the model in Fig. 1 required recasting some of these equations, and re-doing some of the fitting procedures, in terms of model element lengths (L_{CE}, L_{PE}, L_{SE}) instead of L_{M}.

For instance, the activation force–length equation used in Blümel et al. (2012a,b) is

$$F_{\text{L}} = A_{\text{act}} \cdot \left[\frac{1 + \sin\left(\omega \cdot L_{\text{M}} - \left(\frac{\pi}{2} + 2.7 \cdot \omega\right)\right)}{2} \right]. \tag{5}$$

This equation is adequate for the data in Blümel et al. (2012a,b), because in these experiments the measurements were made at steady-state (by which time whatever internal component changes the applied activation induced had been completed) and because the goal of these experiments was only to characterize the muscles sufficiently to make across-individual comparisons. For the muscle model in Fig. 1, however, this equation is inadequate. For instance, consider the situation in which L_{M} is discontinuously changed to a new

value at a constant activation level. In the instant following this change only L_{SE}, not L_{CE}, has changed, and therefore F_L (the force due to the contractile element) has not changed. However, if L_M were used in Eq. 5, it would give a new F_L value. Furthermore, the new F_{SE} slowly causes L_{CE}, and thus F_L, to change (see below). However, if L_M were used in Eq. 5, F_L would incorrectly remain constant. To correctly model contractile element force in dynamic conditions it is therefore necessary to use L_{CE}, not L_M, in Eq. 5 (see also Zajac 1989).

This recasting was achieved by using the equation that relates series elastic element force and length,

$$F_{SE} = k_3 \cdot L_{SE}^2. \tag{6}$$

As explained in Blümel et al. (2012a), because the k_3 values were determined from changes in muscle length, their values are already independent of L_M (it is for this reason that L_{SE}, not L_M, is used in Eq. 6 here and was used in this equation in Blümel et al. 2012a). Because we know each muscle's k_3 value, and because in the model in Fig. 1 muscle output (measured) force equals F_{SE}, we can use muscle force to calculate L_{SE} at all times. Since in the model in Fig. 1 parallel element length always equals contractile element length (in all equations here we abbreviate both these lengths with L_{CE}), and L_{CE} equals L_M minus L_{SE}, we can also therefore at all times calculate L_{CE}.

We used this knowledge of L_{CE} and the data and fitting procedures described in Blümel et al. (2012a) to re-determine the values of the parameters in the Blümel et al. (2012a) equations when expressed in terms of L_{CE}. The first of these equations gives the force of the parallel passive element

$$F_P = k_1 \cdot e^{k_2 L_{CE}}. \tag{7}$$

Table 1 k_1, k_2, and $curv_\omega$ values recalculated in terms of contractile element length instead of total muscle length as was done in Blümel et al. (2012b)

Muscle	k_1 (μN)	k_2 (mm^{-1})	$curv_\omega$
A	1.53	4.87	4.37
B	4.37	4.23	3.65
C	0.71	5.58	4.69
D	4.77	4.30	6.93
E	2.80	4.49	4.70
F	4.06	4.50	6.17
G	1.04	5.27	6.56
H	0.43	6.18	5.49
I	3.90	4.19	4.36
Fold-variation	11.1	1.5	1.9

This recalculation did not substantially alter the fold variations of these parameters and thus does not affect the conclusions of Blümel et al. (2012b)

Recalculating k_1 and k_2 using L_{CE} instead of L_M in all cases reduced k_1 and increased k_2. The k_1 decreases could be as large as 19% and the k_2 increases as large as 3.3% (Table 1). However, these changes either only little (k_1, from 12.9 to 11.1) or did not (k_2) change the across-muscle fold-variation of these parameters, and thus do not alter the conclusions of that work. In the ranges of L_{CE} used here these parameter changes would produce a maximum change in F_P of 0.2%, and F_P was always less than 2% of active force. The correction for L_{CE} in Eq. 6 thus made a negligible difference in model performance.

The next equations describe CE force as a function of muscle activation (act), L_{CE}, and contraction velocity (v):

$$F_L = A_{act} \cdot \left[\frac{1 + \sin\left(\omega \cdot L_{CE} - \left(\frac{\pi}{2} + 2.7 \cdot \omega\right)\right)}{2} \right] \tag{8}$$

where

$$A_{act} = 15 \cdot e^{-1.06.\omega} \tag{9}$$

and

$$\omega = 2.5 + \frac{1}{(curv_\omega \cdot (act + 0.05))^2} \tag{10}$$

$$F_V = \left(e^{-e^{-A\cdot(act-B)}}\right) \cdot \frac{c_{pos} \cdot (1 + c_{pos})}{(v/v_{max\ pos}) + c_{pos}} - c_{pos} \quad \text{(shortening contractions)} \tag{11}$$

where

$$v_{max\ pos} = v_{max(act=1)} \cdot e^{-act/0.3} \tag{12}$$

$$F_V = \frac{c_{neg} \cdot (1 + c_{neg})}{(v/v_{max\ neg}) + c_{neg}} - c_{neg} - \left(1 - e^{-e^{-A\cdot(act-B)}}\right) \quad \text{(lengthening contractions)} \tag{13}$$

In these equations the measurement of only the $curv_\omega$ parameter depended on muscle length and thus had to be re-done. This parameter increased somewhat (Table 1) in all muscles, but this change did not change the across-muscle fold-variation of this parameter. The conclusions of Blümel et al. (2012b) are therefore again not altered by these model-specific recalculations. In contrast to F_P, these changes made substantial (up to 18%) changes in F_L, supporting our decision to recast these equations, and re-determine their parameter values, in terms of L_{CE}.

In the model in Fig. 1 measured muscle force always equals F_{SE} and, because the CE and PE elements are in parallel, F_{SE} always equals and is opposite to the sum of F_{CE} and F_P. It is therefore necessary to know how F_{CE} and F_P vary with component length, activation, and velocity. The F_P

Eq. 7 is straightforward. The CE is more complex, generating force as a function of v, act, and L_{CE}. The F_L (Eqs. 8–10) and F_V (Eqs. 11–13) equations interact to give CE force because the F_L equations give CE force at zero v (the maximum force the muscle can produce at that act and L_{CE}), and the F_V equations give the percentage of this maximum force produced at other v. Multiplying F_L by F_V therefore gives CE force at all v, act, and L_{CE}. Total muscle force opposing F_{SE} thus equals

$$F_L(\text{act}, L_{CE}) \cdot F_V(v) + F_P(L_{CE}) \quad (14)$$

F_{SE} and the force given by Eq. 14 act on the line labeled D dividing the right and left halves of the model. This line moves, and hence L_{SE} and L_{CE} change, whenever these forces are unequal. These movements were calculated using $F = ma$ (with $m = 0.2$ mg, the estimated mass of an extensor muscle) to calculate D's acceleration.

A potential confusion may arise from the parameters in Eqs. 11 and 13 being determined in experiments measuring the velocity of total muscle shortening, whereas the v in the model refers to D line velocity. However, the experimental measurements were taken after the initial, rapid movements were over. L_{SE} would be constant under these conditions, and thus these experiments were measuring D line velocities.

Another model component that had to be added to prevent rapid D line oscillations was a damping element in parallel with CE and PE. These oscillations occurred on the order of model time steps and arose because, in the absence of damping, even very small D line force imbalances caused extremely rapid D line movement. Because muscles do not resist compression, the damping constant was smaller (0.0015 s/mm) when L_{CE} shortened than when it lengthened (0.045 s/mm).

A final issue that had to be dealt with was that the Aurora dual-mode lever system functions as a servo mechanism in which the user inputs a set muscle length and threshold lever force. If muscle force is less than this threshold, muscle length is maintained at the set muscle length (i.e., the Aurora measures the muscle force and delivers not the threshold force, but instead only enough force to keep the muscle at the set length). If muscle force exceeds the threshold, then the Aurora delivers the threshold force to the muscle and allows the muscle to shorten until muscle force equals threshold force. In order to match simulation and experimental conditions, the same constraints were applied to the isotonic simulations.

2.5 Error measurement

Model performance was quantified by calculating the NRMSD of the force or position traces between simulation result and experimental data. In all cases forces were calculated by multiplying normalized force (the intermedi-

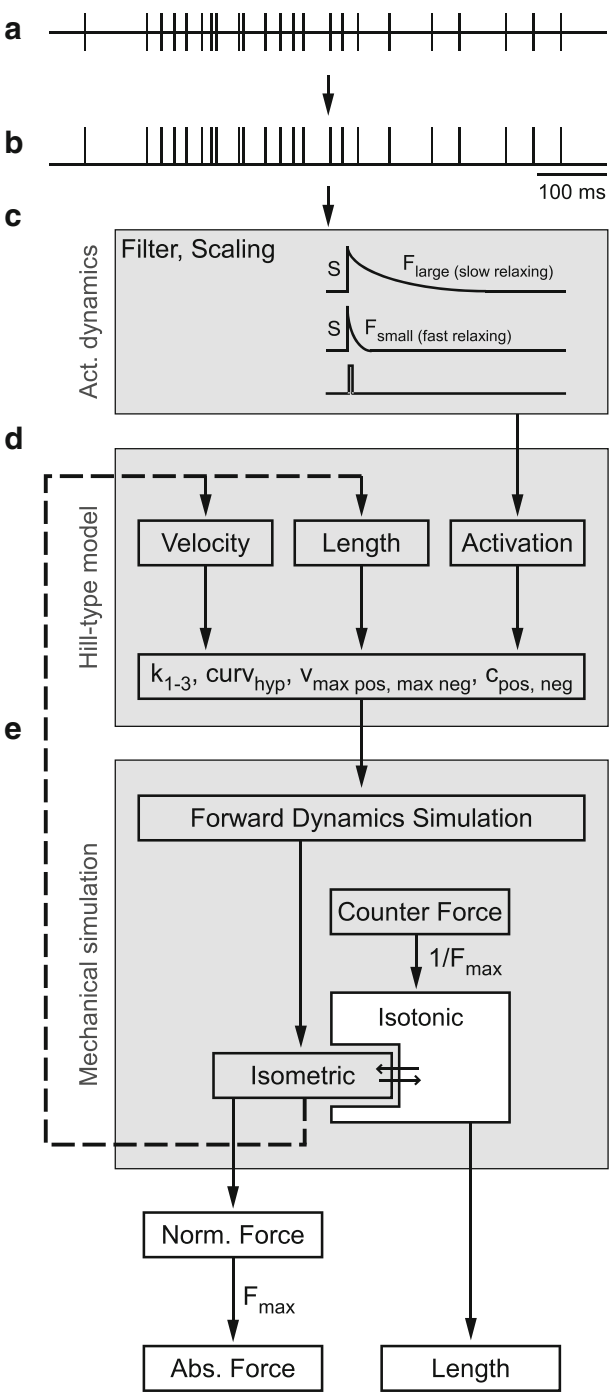

Fig. 2 Model flowchart. Action potentials (*a*) were first converted into pulses of unit amplitude and 1 ms duration (*b*). This pulse sequence was fed into an activation dynamics module (*c*) which converted it into a continuous muscle activation value controlled by two parameters, *scaling* (S) and *filter* (F), that controlled activation amplitude and dynamics, respectively. Muscle activation, the Hill-type equations, and the mechanical model worked together to produce, depending on the experimental condition being modeled, isometric or isotonic contractions (*d*, *e*). For isotonic contractions experimental counterforce was normalized to each muscle's F_{max}, and thus simulation and experimental movements could at this stage be directly compared. For isometric contractions the simulation's normalized force output was multiplied by each muscle's F_{max} to allow comparison to experimental data

ate model output, see Fig. 2) by either mean F_{max} (for the all-mean and F_{max}-mean cases) or muscle-specific F_{max} (for muscle-specific and F_{max}-specific cases) (see Sect. 3 for definition of these cases). Error is expressed as percent in all figures and tables. Error bars in Figs. 5 and 6 are standard deviations; means were compared with either repeated measures ANOVA or matched Student's t test in Kaleidagraph (Synergy Software, Reading, PA).

2.6 Computational methods

Calculations were performed in GnuOctave on Linux (Ubuntu 9.04, Kernel 2.6.28-15-generic, Intel Core2 T5600). Parameters were optimized using the *leasqr* routine of the *optim* package (version 1.0.12). Numerical integration was implemented using second order "improved Euler" as described in Boug (2001) and a Runge-Kutta type 2 correction. NRMSD values were calculated with custom code.

3 Results

3.1 Model summary

Testing whether using muscle-specific parameter values significantly reduced muscle simulation error required a muscle model (Figs. 1, 2; see Sect. 2 for detailed explanation). We first used threshold detection to transform neural spiking input (Fig. 2a) into 1 ms duration impulses of amplitude 1 (Fig. 2b). Each impulse induced a change in muscle activation that was controlled by two parameters, *scaling* (S), which determined activation per impulse amplitude and *filter* (F), which determined how quickly activation decayed (Fig. 2c) (different *filter* values were used for isotonic and isometric contractions, see Sect. 3.4). Contractile element force changed with activation and, in conjunction with the model's Hill-type (Fig. 2d) and mechanical (Fig. 2e) modules, generated forces at, and movements of, the D line in Fig. 1. In isometric contractions these movements stretched the series elastic spring and fed back to the Hill-type module. Since the model worked with forces normalized to F_{max}, the maximum force the muscle produced at rest length, simulation output was then multiplied by F_{max} to compare it to muscle data. In isotonic contractions D line movements resulted in changes in total muscle length if the isometric force was greater than the counter force, where counter force was normalized to F_{max}.

3.2 Muscle model configurations

We tested the effects of across-muscle parameter averaging in four model configurations (Fig. 3). In the first (a) muscle activation dynamics, Hill parameters, and F_{max} were all simulated using muscle-specific values. In the second (b) across-muscle mean values (with separate *filter* means for isotonic and isometric contractions; see Sect. 3.4) were used for all model components. The third and fourth cases investigated the importance of F_{max} by using mean values for muscle activation dynamics and Hill parameters and muscle-specific F_{max} values (c) or muscle-specific values for muscle activation dynamics and Hill parameters and the across-muscle F_{max} mean (d).

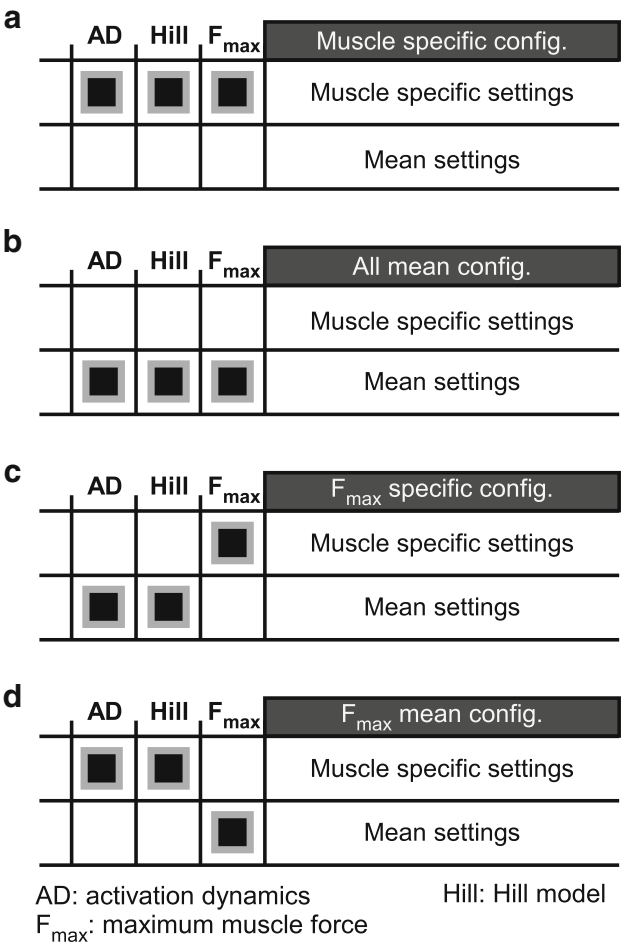

Fig. 3 Overview of simulation configurations. Simulations were run with: **a** muscle-specific values for activation dynamics, Hill parameters, and F_{max}, **b** across-muscle means of all these model components, **c** mean values for activation dynamics and Hill parameters but muscle-specific F_{max} values, and **d** muscle-specific values for activation dynamics and Hill parameters but the across-muscle mean F_{max} value

3.3 Activation dynamic terms did not depend on stimulation frequency

Because they are not part of the standard Hill-type muscle description, the activation dynamic terms *filter* and *scaling* were not measured in our prior work (Blümel et al. 2012a,b). We therefore determined the values of

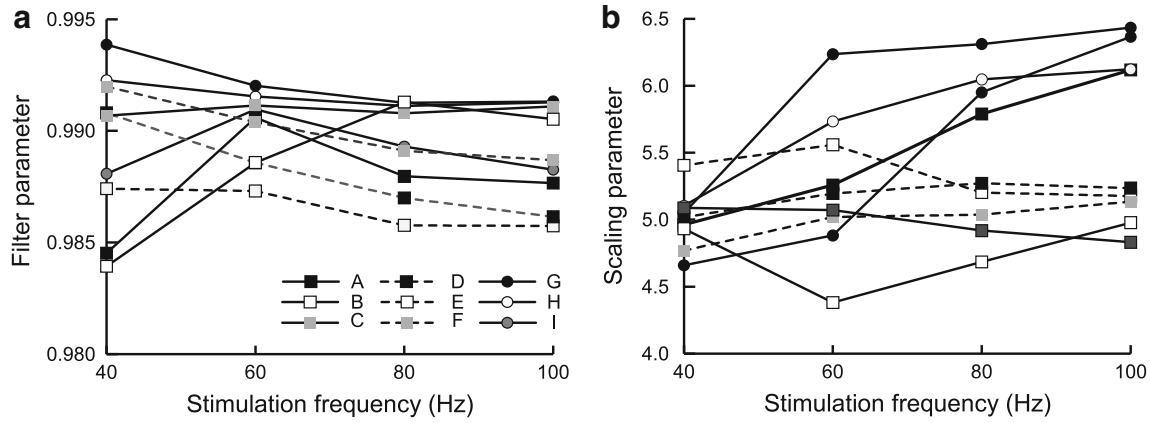

Fig. 4 *Filter* and *scaling* did not depend on stimulation frequency. *Filter* and *scaling* were optimized to tonic stimulations at multiple frequencies (40, 60, 80, and 100 Hz; all isometric contractions). **a** No systematic dependence of *filter* on frequency was present. **b** *scaling* plotted over same four stimulation frequencies. Across-muscle variation was greater than for the *filter* parameter, but again no systematic dependence on stimulation frequency was present. Key identifies from which muscle the data are from and applies to both panels

these parameters here as described in this and the next section. The first step was to determine if the parameters depended on stimulation frequency, as has been observed in the locust (Zakotnik 2006; Zakotnik et al. 2006). This possibility was tested by optimizing *filter* and *scaling* at each of the four fixed frequency (40, 60, 80, and 100 Hz) stimulations applied to the muscles (see Sect. 2.1). *Filter* values ranged from 0.984 to 0.994 and did not consistently vary with stimulation frequency (Fig. 4a). *Scaling* had much greater across-muscle variation than *filter* (1% for *filter* vs. 40% for *scaling*) (Fig. 4) but again did not consistently vary with stimulation frequency. In the simulations we therefore used the across-frequency means of each muscle's *filter* and *scaling* parameter data, with muscle-specific or across-muscle means being used depending on which case in Fig. 3 was being investigated.

3.4 Activation dynamics differed in isometric and isotonic contractions

The observation that *filter* and *scaling* did not depend on spike frequency in fixed-frequency isometric contractions did not prove that these parameters would not have different values in physiological isometric contractions or in isotonic contractions. To examine this issue we fit *filter* and *scaling* in all stimulation and contraction conditions in all muscles (Fig. 5; this figure thus contains the fit values in Fig. 4—the 'isometric: fixed frq' data—and the fits to isometric and isotonic contractions in response to physiological motor nerve stimulations). Fits of the *filter* parameter showed only small stimulation condition and inter-muscle variation (range 0.973–0.994, a 2% change) (Fig. 5a). Most of this variation appeared to be not due to across-muscle variation in isometric values, but instead to *filter* being less in isotonic contractions. Statistical comparisons (bar graphs, right) confirmed this impression. There was no difference between the mean *filter* values of the fixed frequency (bar 1) and physiological (bar 2) stimulation isometric contractions (both means 0.99; $p = 0.65$, paired Student's t test). The mean *filter* values of the physiological isometric (bar 2) and isotonic (bar 4) contractions, however, did differ (respective means 0.99 ± 0.002; 0.98 ± 0.004; $p = 0.0006$, paired Student's t test). Isometric simulations were therefore modeled with the mean of all the isometric *filter* values (0.99, bar 3) and isotonic simulations with the mean of the isotonic (only physiological stimulations) *filter* values.

Scaling showed much greater stimulation condition and inter-muscle variation (range 2.6–6.5, 2.5-fold) (Fig. 5b). Most of this variation was again because of *scaling* being smallest in isotonic conditions (3.4 ± 0.22, bar 4). This mean differed from the mean under isometric physiological conditions (4.5 ± 0.37, bar 2; $p < 0.0001$, paired Student's t test), and was therefore used in all isotonic simulations. *scaling* was also consistently smaller ($p = 0.0004$, paired Student's t test) in physiological (bar 2) than fixed frequency (5.33 ± 0.4, bar 1) isometric contractions. However, the lack of dependence of *scaling* on spike frequency in the fixed frequency stimulations (Fig. 4b) meant that we could not incorporate this difference into the modeling parametrically, and we were unwilling to use different *scaling* values simply on the basis of the stimulation pattern being fixed-frequency versus physiological. We therefore modeled all isometric simulations using the mean of the fixed-frequency and physiological isometric *scaling* values, 4.91 ± 0.57 (bar 3).

Measuring these activation dynamics parameters raised the question of whether they correlated with across-muscle changes of the other muscle-describing parameters, a major

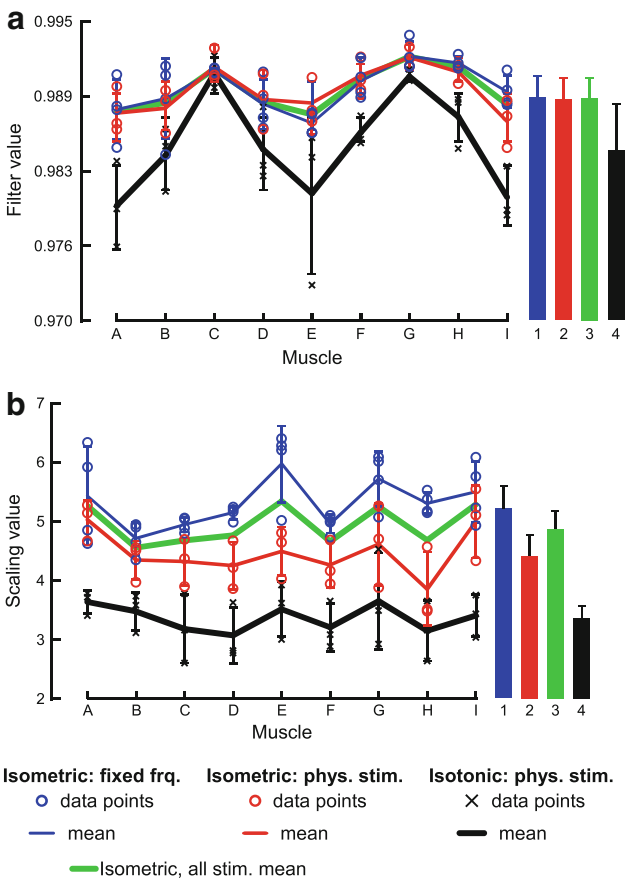

Fig. 5 The activation dynamics parameters *filter* (**a**) and *scaling* (**b**) showed greatest differences as a function of whether the contractions were isometric or isotonic. Figure construction is identical in both *panels*. In the individual muscle portion of the panels (columns labeled A–I) *blue circles* denote parameter values calculated from fixed (tonic) motor nerve stimulations under isometric conditions, *red circles* parameter values calculated from physiological motor nerve stimulations under isometric conditions, and *black cross's* parameter values calculated from physiological motor nerve stimulations under isotonic conditions. The *lines* (*blue*, *red*, and *black*) connect each paradigm's mean parameter values across muscles. The *green line* connects the means of the two isometric conditions. In the averaged portion of the *panels* (*right*) *each bar* shows all-muscle means with the following code: *1* fixed (tonic) motor nerve stimulations under isometric conditions, *2* physiological motor nerve stimulations under isometric conditions, *3* all isometric conditions, *4* all isotonic conditions. In both portions error bars are standard deviations. Statistical comparisons are reported in Sect. 3.4. (Color figure online)

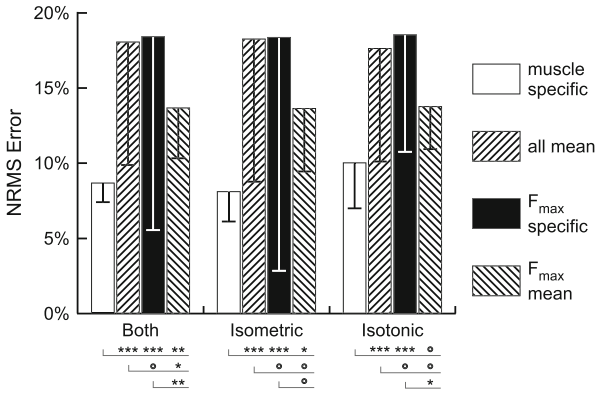

Fig. 6 Error (NRMSD, in percent) comparison of using different combinations of muscle-specific and mean parameter values. The muscle-specific models (first bars in each group) were best both when all contraction types were averaged together (group of bars labeled 'Both') and when isometric and isotonic contractions were averaged individually. Using either mean values for all model parameters (second bars in each group) or F_{max} muscle-specific and mean Hill values (third bars in each group) approximately doubled simulation errors. Using mean F_{max} and muscle-specific Hill values (fourth bar in each group) gave intermediate errors. Error bars are standard deviations. *Lines and asterisks under bars* in each group show statistical comparisons, with *vertical lines* showing which mean is being compared to the others and *triple asterisks* being $p < 0.001$, *double asterisks* being $0.001 \leq p < 0.01$, *single asterisk* being $(0.01 \leq p < 0.05)$, and *open circles* being $p \geq 0.05$ in a repeated measures ANOVA

part of Blümel et al. (2012b). Repeating this analysis showed that the two parameters did not significantly co-vary with each other or any other parameter.

3.5 Model performance with muscle-specific parameter values

With muscle-specific parameter values simulation NRMSD error ranged from 5.4% (muscle F, isometric contractions) to 17.3% (muscle C, isotonic contractions), with an all-condition and all-muscle mean of $8.7 \pm 1.4\%$ (first column, 'Both' data in Fig. 6; Table 2). Isometric and isotonic contraction mean errors (first columns, 'Isometric' and 'Isotonic' data in Fig. 6; Table 2) did not differ ($p = 0.13$, unpaired Student's t test assuming unequal variance).

Table 2 Simulation performance of all muscles

Condition	A	B	C	D	E	F	G	H	I	Mean
IM and IT	9.8	10.7	10.0	7.6	8.7	6.3	7.6	9.3	8.0	8.7 ± 5.1
IM	11.0	11.1	6.9	5.5	8.9	5.4	6.7	9.2	8.3	8.1 ± 4.9
IT	7.0	10.0	17.3	12.6	8.3	8.5	9.7	9.5	7.3	10.0 ± 5.5

The first row shows the mean error of all conditions (isometric and isotonic), the second the mean error of only the isometric simulations, and the third the mean error of only the isotonic simulations. All errors are expressed as normalized root mean square deviations (NRMSD) in percent. The last column shows the overall mean of each row

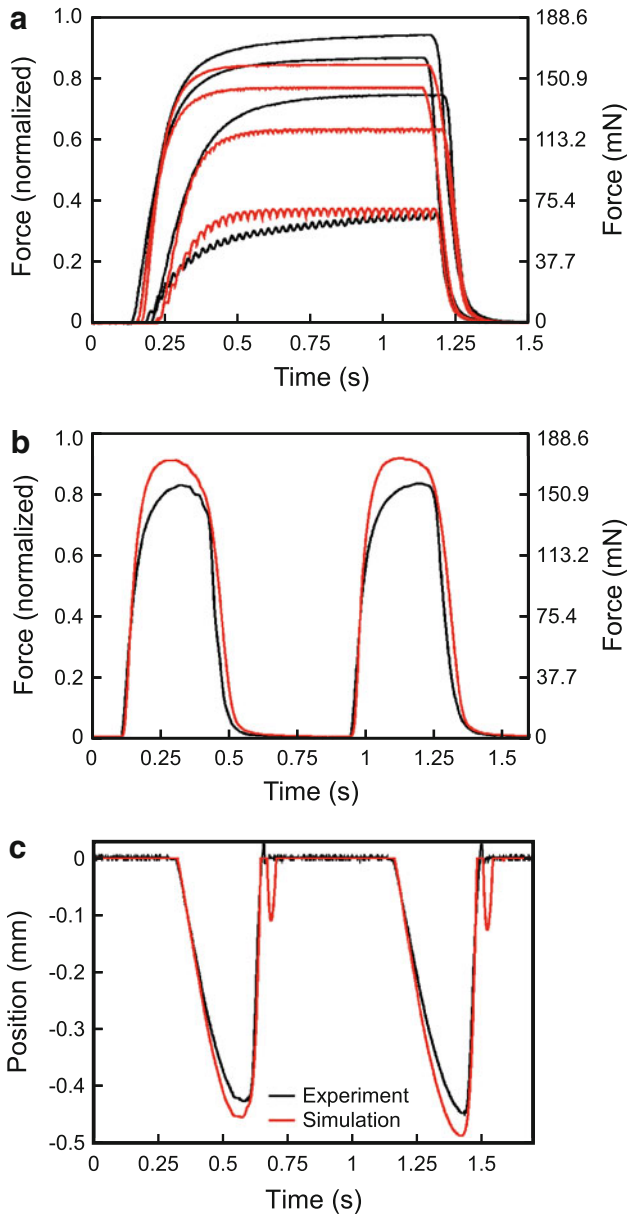

Fig. 7 Simulation results of a muscle (E) with a mean error close to the across-muscle mean error ('mean' column, row 1, Table 2). **a** Experimental data and simulation output of isometric contractions in response to fixed-frequency motor nerve stimulations at 40, 60, 80, and 100 Hz. **b** Experimental data and simulation output of isometric contractions in response to motor nerve stimulations with physiological stimulation pattern 2. **c** Experimental data and simulation output of isotonic contractions in response to motor nerve stimulations with physiological stimulation pattern 2. In all panels *black lines* are experimental data and *red lines* simulation output. (Color figure online)

To provide a visual impression of how well simulations with this level of error reproduced the experimental data, Fig. 7 shows simulations for muscle E, whose isometric and isotonic errors were nearest the all muscle mean values (Table 2). Panel a compares simulations (red) and experimental data (black) of the four fixed-frequency isometric contractions. The real contractions were characterized by an initial rapid force increase whose slope increased with increasing motor nerve stimulation frequency, a later slow increase that continued throughout the stimulation, and an exponential force decline at stimulation end. The simulations well reproduced the rapid initial rise for the high frequency stimulations but not for the 40 Hz case, in which a trade-off occurred with a too-fast rise starting too late in the motor neuron burst. The amplitude of the lowest frequency simulation was too large throughout most of the contraction and the amplitudes of the other frequency simulations were too small. None of the simulations reproduced the late slow force increase of the real data. The time courses of the exponential relaxations at stimulation end were well reproduced. Panels b and c show isometric and isotonic responses to physiological stimulation pattern 2. In both cases the rise and fall phases of the contractions were well reproduced, with the primary error source being inaccurate simulation amplitudes. The isotonic (Panel c) simulations shown here also had a late, small, transient shortening not present in the real muscle that was an artifact of the muscle model's internal damping and was, of all the muscles simulated, largest for the muscle (E) shown here.

Examination of the simulations for the other muscles showed that the error sources in all muscles were similar. In particular, in no cases could the model reproduce the late slow components of the fixed frequency contractions. Difficulties reproducing the rise phase of the 40 Hz contractions were also common. The remaining errors were typically due to a failure to reproduce contraction amplitudes, although which stimulation conditions had incorrect amplitudes varied from muscle to muscle.

3.6 Comparison to performance with across-muscle means

We investigated the effects of using muscle-specific versus mean parameter values in four configurations (Fig. 3): all parameters muscle-specific, all parameters mean, F_{max} muscle-specific and Hill parameters mean, and F_{max} mean and Hill parameters muscle-specific. We present these data both as mean errors of the combined isometric and isotonic simulations (group of bars labeled 'Both' in Fig. 6) and as mean errors of only the isometric or only the isotonic simulations (groups of bars labeled 'Isometric' and 'Isotonic' in Fig. 6).

Using muscle-specific parameter values always produced the smallest mean errors (first bars in each group, Fig. 6). Using across-muscle mean values (second bars in each group) approximately doubled simulation error both in the all-contraction comparisons and when isometric and isotonic contractions were analyzed separately (in all cases the increase was significant at $p < 0.001$, repeated measures ANOVA). Using muscle-specific F_{max} values and mean Hill

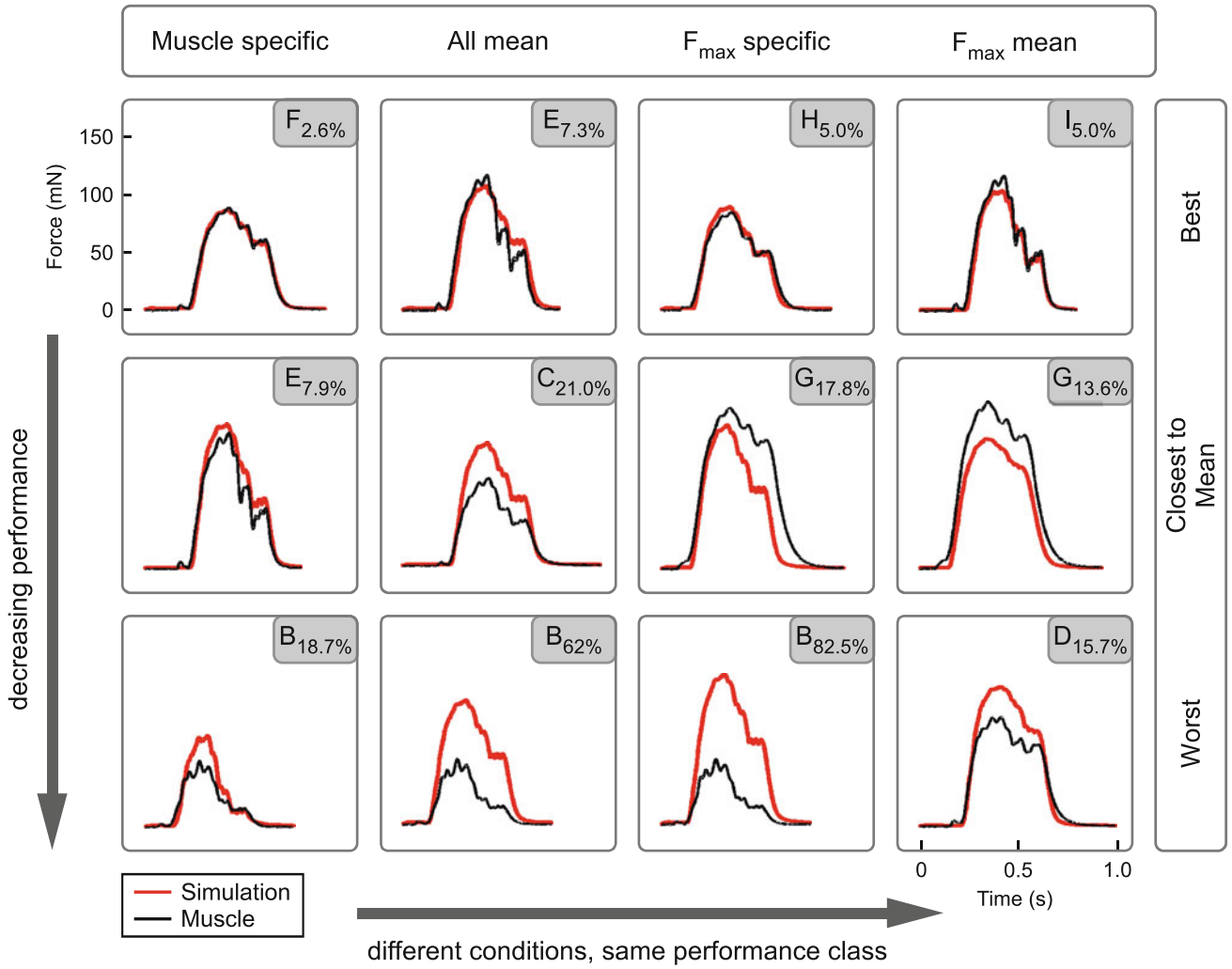

Fig. 8 Exemplary contractions showing how error increased in each combination of muscle-specific and mean parameter values used in the simulations, and the effects of changing these combinations. This figure shows 12 isometric contractions, each induced by physiological simulation pattern 1. Each column shows one of the four model configurations. The first row shows the best performing contraction of each condition, the second the contraction closest to the mean error of all muscles, and the third the worst performing simulation. Comparing the plots in each column thus shows how much variation there is inside a single model configuration. Comparing the plots across a row shows how the different configurations vary in the same performance class (best, mean, worst). In all panels *black lines* are experimental data and *red lines* simulation output. (Color figure online)

parameter values (third bars in each group) did not change simulation error. Using mean F_{max} values and muscle-specific Hill parameter values (fourth bars in each group) decreased simulation error in all cases, although, depending on the comparison being made, these decreases were not always significant. These decreased errors were, however, still always larger than the errors using muscle-specific values for all parameters, with this difference being significant in both the all-contraction and isometric contraction comparisons.

The data in Fig. 6 are from 360 simulations (10 motor nerve stimulation conditions per muscle times 4 combinations of parameter values times 9 muscles). It is clearly impossible to show all these data. We instead show examples only of the simulations with least, closest-to-mean, and greatest error (rows, Fig. 8) for each combination of parameter values (all parameter values muscle-specific, all parameter values averaged, F_{max} muscle-specific and Hill parameter values averaged, and F_{max} values averaged and Hill parameters muscle-specific, columns 1–4, respectively, Fig. 8), all of isometric contractions induced by the single-step physiological stimulation pattern 1. The traces in each column therefore illustrate how model performance can vary within a particular combination of muscle-specific and mean parameter values. The traces in each row, alternatively, show the effects of changing which combination is being used. The selected muscle and its error are noted in the upper right corner of each plot.

A first important point to make about these plots is the large diversity of contractions that the different muscles produced in response to the identical motor nerve stimulations (see also Fig. 1 in Blümel et al. 2012a; Hooper et al. 2006). This great across-muscle variation formed a large part of the motivation to attempt muscle-specific descriptions and modeling, as any single muscle model (which any model made from averaged data must be) would of course always produce identical output for identical input, and thus could not reproduce this inter-muscle variability.

Increasing error in the muscle-specific models was primarily due to an increasing overestimation of force. In the second column the simulations all had identical parameter values, and thus model output was identical in all plots. The overall shape of the model output reasonably well reproduced the three step nature of the muscle contractions, with an initial large first peak following by two steps of sequentially decreasing amplitude. Error arose because of the variability in force production across muscles. Using muscle-specific F_{max} and mean Hill parameter values (column 3) or vice versa (column 4) again reproduced relatively well the overall shape of the real contractions, with error again increasing primarily because of errors in overall force levels.

4 Discussion

4.1 Summary of data presented here

We built a muscle model and used stick insect extensor muscle data to determine the values of the model's activation dynamic parameters. These parameters, at least in isometric contractions, did not depend on stimulation frequency, but did differ in isometric and isotonic contractions. We then showed that simulations using muscle-specific parameters had approximately half the error (8.7 vs. 18.1%) of simulations using either across-muscle mean parameter values or muscle-specific F_{max} values with across-muscle mean Hill-type parameter values, and that using across-muscle F_{max} values with muscle-specific Hill-type parameter values gave intermediate errors (13.7%). These data indicate that most accurate modeling of stick insect extensor muscle contractions requires using muscle-specific parameter values.

4.2 Which parameters must be muscle-specific for low simulation error?

It is unfortunate that using muscle-specific F_{max} values with across-muscle mean Hill-type parameter values did not result in low-error simulations, as F_{max} is particularly simple to measure. Our data should not, however, be interpreted to mean that it is necessary to use muscle-specific values for all model parameters. The analysis presented here is sufficient only to state that F_{max} and at least some subset of the other parameters must be muscle-specific for accurate modeling. This issue could be examined for all parameters by sequentially running the simulations using in each run the mean value for one parameter and muscle-specific values for the rest (exactly analogous to the analysis we performed with F_{max}). We did not perform these analyses on the model's other 10 parameters because (1) once one begins to measure some of the Hill-type parameters it is not much additional work to measure them all, (2) the large variations present in all the Hill-type parameters and lack of correlated changes among them suggests that they may all contribute to simulation performance, and (3) sufficient error remains in the model (see next section) that analysis on this level of detail seemed premature.

4.3 Use of different activation dynamic values in isometric versus isotonic contractions

A notable characteristic of the model is that it works equally well at simulating isometric and isotonic contractions (the difference between the two errors in Table 2 is not significant, $p = 0.13$, Student's t test assuming unequal variance). Simulations run using the isometric *filter* and *scaling* values in the isotonic contraction simulations, isotonic values in the isometric simulations, or mean values in both contraction types always resulted in substantial error increases (data not shown). As such, at least in stick insect extensor muscles, measuring activation dynamics separately for isometric and isotonic contractions is essential to construct accurate muscle models. We do not suggest detailed hypotheses for why these values should differ in the two contraction types. However, differences at the level of the actomyosin might be assumed not to play a major role, as the model's F–L and F–V equations should function equally well whether the muscles are shortening or not. An alternative source that could play a major role is the very large titin-like proteins present in muscles, whose lengths might change differently in shortening (isotonic) versus fixed-length (isometric) contractions, and thus alter contraction characteristics in the two contraction types. An additional source may stem from muscles being fixed-volume entities, and thus their diameter having to change when their length changes. Such changes in gross muscle shape might also result in changes in contraction characteristics in fixed-length versus shortening contractions.

4.4 Sources of remaining error

The large numbers of muscles, stimulation types, and contractions conditions performed in this work allowed us to perform detailed error comparisons. Because of their clear superiority, we performed these detailed comparisons on only

the muscle-specific simulations. This work showed that the mean errors reported in Table 2 are skewed by the presence of a long tail with high errors (e.g., the 18.7% error simulation in Fig. 8, column 1, row 3). The effect of this tail is shown by the median error across all stimulations being only 6.9%. This work also showed that all muscles were equally well simulated (i.e., there were no significant differences between the errors across muscles in any row in Table 2).

Examination of the different stimulation conditions showed that the isotonic simulations using physiological stimulation pattern 1 had significantly greater error than any other condition except for the isometric 40 Hz simulations, and that the isometric 40 Hz simulations had greater error than the 80 and 100 Hz isometric simulations, the isometric simulation of physiological stimulation pattern 3, and the isotonic simulation of physiological stimulation pattern 2 (repeated measures ANOVA). Physiological stimulation pattern 1 had a much lower mean spike frequency in the motor neuron burst (76 ± 53 Hz) than patterns 2 (187 ± 69) and 3 (128 ± 76) (all different from one another at $p < 0.0065$ or better, ANOVA). Taken together, these data suggest that the model is less accurate at low-frequency simulations.

Two lines of evidence suggest that much of this error is due to our very simple activation dynamics. First, when the simulations are run with each stimulation condition's individual best *filter* and *scaling* values (the data points in Fig. 5) simulation error drops to a mean of only $5 \pm 0.6\%$. We could not take advantage of these stimulation condition differences in *filter* and *scaling* values because we could not find (Fig. 4) any parametric explanation for their variation. Nonetheless, this great improvement in model performance suggests that this variation underlies close to half the simulation's present errors. Second, examination of the 40 and 60 Hz fixed frequency stimulations show in some muscles clear changes in contraction force amplitude early in the stimulation that may be due to facilitation or similar history-dependent effects. Our data are insufficient to model these changes, but an obvious first step in improving this aspect of the model would be a detailed examination of *filter* and *scaling* dependence on spike history.

The second clear systematic source of error was the failure of the model to reproduce the late, slow force increase that continues throughout motor nerve stimulation in the isometric fixed-frequency contractions (Fig. 7a). Model rise dynamics result primarily from the dynamics of the low-pass activation filter used here (Sect. 2.4). This filter has only a single time constant, and thus can only produce contractions with a single time constant. It consequently cannot reproduce the multiple time constants contained in the initial rapid and subsequent slow rise seen in the real contractions. The extensor muscle is innervated by two excitatory motor neurons, one of which primarily activates fast-contracting muscle fibers and the other of which primarily slow-contracting fibers, and in our stimulations both motor axons were activated. The late, slow contraction thus likely arose from activation of extensor slow muscle fibers. In the stick insect it is difficult to activate these motor axons separately, and hence we were unable to perform this work using only one muscle fiber type. In the locust, alternatively, these motor axons are carried in different nerves (Campbell 1961). Repetition of the work reported here in locust would thus allow testing of our approach without this confounding factor.

4.5 General relevance

Given the great improvement in model performance shown here for the stick insect extensor muscles, these data suggest that using the methods presented here and in Blümel et al. (2012a,b) to construct individual muscle-specific models may be also advantageous in other systems. An important point in this context is that dynamic simulations have become an increasingly important tool both for testing motor control hypotheses and for developing new ones (Pearson et al. 2006; Grillner 2003; Siebert et al. 2008). For both goals it is crucial to be able to separate the roles of neural control and muscle properties in the generation of behavior (Ekeberg et al. 2004; Ekeberg and Pearson 2005; von Twickel et al. 2011). For example, during stance phase in walking, load sensory input increases stance motor neuron activity (i.e., 'reinforces' the simultaneously occurring centrally driven stance motor neuron activity). However, leg velocity changes as stance progresses (e.g., leg velocity is lowest at stance beginning). Muscle force–velocity curves are such that, at a given activation level, muscles develop more force at lower velocities. Thus, the increase in muscle activation from the load sensory feedback, if unaltered as stance proceeds, would induce smaller and smaller increases in muscle force as leg velocity increases (Bässler 1988; Pearson and Collins 1993; for reviews see, Clarac et al. 2000; Büschges et al. 2008). Neural and muscle based mechanisms in load-induced reinforcement therefore presumably change in a complicated manner throughout stance. Highly accurate muscle modeling is likely important in resolving this and similar situations in which neural and muscle mechanisms interact.

More generally, our data provide another example of the great individual-to-individual variation present in natural populations, and the importance of taking this variation into account when examining biological phenomena (see, for instance, Golowasch et al. 2002; Hooper et al. 2006; Langlois and Roggmann 1990; Prinz et al. 2004). In retrospect the failure of averaging implied by this and the present work is not surprising-in a system with ten independently assorting parameters, even if for each parameter 50% of the population had the mean value, only $0.5^{10} = 0.1\%$ of the population's individuals would have mean values for all ten. This does not mean that all parameter combinations are necessarily pres-

ent in a population, as combinations that have too deleterious an effect would either fail during development or early life or be prevented by the evolution of appropriate genetic regulation. Nonetheless, it is clear that muscles and effectors show great across-population variation (e.g., human height and strength variation). This variability is presumably evolutionarily acceptable because the great inherent flexibility of nervous systems and their ability to learn allow them to make compensatory changes in their outputs so as to maintain functional behaviors.

This ability to compensate suggests that nervous systems and their effectors may be able to show particularly large across-individual variation and still maintain acceptable function. If so, the data we present here, and those of the other workers noted above showing similar large variation, suggest that averaging may be particularly inappropriate in neuroscience and biomechanics. Modern techniques and computer resources make the sort of individual-specific measurements and modeling presented here and in Blümel et al. (2012a,b) increasingly possible. The great across-individual variability seemingly present in these systems suggests that such individual-specific approaches may be required to fully understand how nervous systems generate behavior.

Acknowledgments Research supported by a Mercator Guest Professor award to SLH and grant Bu857/9 to AB, both from the Deutsche Forschungsgemeinschaft.

References

Bässler U (1988) Functional principles of pattern generation for walking movements of stick insect forelegs: the role of the femoral chordotonal organ afferences. J Exp Biol 136:125–147

Blümel M, Hooper SL, Guschlbauer C, White WE, Büschges A (2012a) Determining all parameters necessary to build Hill-type muscle models from experiments on single muscles. Biol Cybern 106:543–558 doi:10.1007/s00422-012-0531-5

Blümel M, Guschlbauer C, Gruhn S, Hooper SL, Büschges A (2012b) Hill-type muscle model parameters determined from experiments on single muscle show large animal-to-animal variation. Biol Cybern 106:559–571 doi:10.1007/s00422-012-0530-6

Boug DM (2001) Physics for Game Developers. O'Reilly Media, Cambridge, MA

Büschges A, Akay T, Gabriel JP, Schmidt J (2008) Organizing network action for locomotion: insights from studying insect walking. Brain Res Rev 57:162–171

Campbell JI (1961) The anatomy of the nervous system of the mesothorax of *Locusta migratoroides* R & F. Proc Zool Soc Lond 137:402–432

Clarac F, Cattaert D, Le Ray D (2000) Central control components of a 'simple' stretch reflex. Trends Neurosci 23:199–208

Ekeberg O, Pearson KG (2005) Computer simulation of stepping in the hind legs of the cat: an examination of mechanisms regulating the stance-to-swing transition. J Neurophysiol 94:4256–4268

Ekeberg O, Blümel M, Büschges A (2004) Dynamic simulation of insect walking. Arthropod Struct Dev 33:287–300

Golowasch J, Goldman MS, Abbott LF, Marder E (2002) Failure of averaging in the construction of a conductance-based neuron model. J Neurophysiol 87:1129–1131

Grillner S (2003) The motor infrastructure: from ion channels to neuronal networks. Nat Rev Neurosci 4:573–586

Hatze H (1977) A myocybernetic control model of skeletal muscle. Biol Cybern 25:103–119

Hatze H (1978) A general myocybernetic control model of skeletal muscle. Biol Cybern 28:143–157

Hooper SL, Guschlbauer C, von Uckermann G, Büschges A (2006) Natural neural output that produces highly variable locomotory movements. J Neurophysiol 96:2072–2088

Hooper SL, Guschlbauer C, von Uckermann G, Büschges A (2007) Slow temporal filtering may largely explain the transformation of stick inect (*Carausius morosus*) extensor motor neuron activity into muscle movement. J Neurophysiol 98:1718–1732

Langlois JH, Roggmann LA (1990) Attractive faces are only average. Psychol Sci 1:115–121

Pearson KG, Collins DF (1993) Reversal of the influence of group Ib afferents from plantaris on activity in medial gastrocnemius muscle during locomotor activity. J Neurophysiol 70:1009–1017

Pearson KG, Ekeberg O, Büschges A (2006) Assessing sensory function in locomotor systems using neuro-mechanical simulations. Trends Neurosci 29:625–631

Prinz AA, Bucher D, Marder E (2004) Similar network activity from disparate circuit parameters. Nat Neurosci 7:1345–1352

Siebert T, Rode C, Herzog W, Till O, Blickhan R (2008) Nonlinearities make a difference: comparison of two common Hill-type models with real muscle. Biol Cybern 98:133–143

Smith SW (1997) The scientist and engineer's guide to digital signal processing. California Technical Publishing, San Diego, CA

von Twickel A, Büschges A, Pasemann F (2011) Deriving neural network controllers from neuro-biological data: implementation of a single-leg stick insect controller. Biol Cybern 104:95–119

Winters JM (1990) Hill-based muscle models: a systems engineering perspective. In: Winters JM, Woo SLY (eds) Multiple muscle systems: biomechanics and movement organization. Springer, New York pp 69–93

Zajac FE (1989) Muscle and tendon: properties, models, scaling, and application to biomechanics and motor control. Crit Rev Biomed Eng 17:359–411

Zakotnik J (2006) Biomechanics and neural control of targeted limb movements in an insect. PhD thesis, Universität Bielefeld

Zakotnik J, Matheson T, Dürr V (2006) Co-contraction and passive forces facilitate load compensation of aimed limb movements. J Neurosci 26:4995–5007